Diagonal scan measurement of Cr:LiSAF 20 ps ablation threshold

Ricardo Elgul Samad,* Sonia Licia Baldochi, and Nilson Dias Vieira, Jr.

Centro de Lasers e Aplicações—Instituto de Pesquisas Energéticas e Nucleares, IPEN—CNEN/SP, Av. Prof. Lineu Prestes, 2242—Cidade Universitária—CEP 05508-000 São Paulo, Brazil

*Corresponding author: resamad@gmail.com

Received 14 December 2007; accepted 20 December 2007;
posted 3 January 2008 (Doc. ID 90841); published 28 February 2008

We report the measurement of the 20 ps ablation threshold of pure and Cr^{3+} doped LiSAF samples using a simple method that employs a single scan of the sample across a focused laser beam waist. During the scan, a profile is etched in the sample surface, and the measurement of the maximum transversal size of the profile and the pulse peak power determine the ablation threshold, without any further knowledge of the beam geometry. Also, it was possible to measure the depth of the ablation profile, to calculate its effective volume, and to identify that the maximum material removal rate per pulse does not occur at the beam waist, which is not intuitively expected. © 2008 Optical Society of America

OCIS codes: 320.5390, 320.7120, 320.7130, 140.3390, 220.4610.

1. Introduction

Ultrashort pulse laser ablation of solids is due to an electron avalanche induced breakdown process [1,2], which occurs when seed electrons are accelerated in the laser field, exponentially generating free electrons by collisions. The breakdown takes place when the plasma originated by the avalanche electrons reaches a critical density and transfers energy to lattice ions, which expand away from the surface after the pulse has passed. In metals, the seed electrons are always present (conduction band free electrons), and in dielectrics and semiconductors they are excited from the valence band to the conduction band by the pulse leading edge, either by multiphoton ionization [3,4] or by tunneling induced by the laser field [5–7]. Although the seed electrons have dissimilar origins in different kinds of material, a metallization occurs in dielectrics and semiconductors after they are produced, and the avalanche evolves deterministically in time [2,8,9] in the same way in all solid materials that now behave like metals [10,11]. These mechanisms confer a nonselective characteristic to the ultrashort pulse ablation, and the intensity ablation threshold of a material, I_{th}, is the only parameter relevant to the etching process.

The established method [12] to determine the ablation threshold of a given material consists of ablating the material using a TEM_{00} Gaussian beam at various intensities in different positions on the sample surface, and then measuring each ablation area diameter. A function fit to the area diameter dependence on the intensity provides the ablation threshold [12]. The method requires the knowledge of all the geometrical experimental parameters (lens focal length, sample relative position to the lens, and beam propagation law), the pulses' energies, and a series of measurements, and can be applied to pulse durations under tens of picoseconds.

In a previous work, we analytically described an alternative method to determine the ablation threshold in the ultrashort regime [13], based in the very precise definition of the etching region resulting from the nonlinear character of the ultrashort pulse ablation together with the almost inexistent lateral heat diffusion. If lattice heating occurs, the diameter of the ablated area will depend on the material thermal properties, and the method can no longer be used. Here we present the results of applying the method

0003-6935/08/070920-05$15.00/0
© 2008 Optical Society of America

to Cr:LiSAF samples in the 20 ps regime. The temporal pulse width and samples were chosen due to their utilization in ultrashort pulse amplification and our experience in growing fluoride crystals [14,15].

2. Diagonal Scan Method and Experimental Setup

The method developed by us, which is schematized in Fig. 1(a), consists of scanning a solid sample diagonally across the beam waist of a focused laser beam. The sample starts in a position where there is no ablation, and then it is moved simultaneously in the z and y directions passing through the beam focus, up to the point where the ablation has ceased. This diagonal scan (D-Scan) etches a profile in the sample surface. If the pulse power is above the critical power [13] $P_{\text{crit}} = (1/2)e\pi w_0^2 I_{\text{th}}$, the etched profile will be similar to the one shown in Fig. 1(b), presenting two lobes, and in this case a simple equation relating the half maximum transversal dimension of the profile, $\rho_{\max}$, the pulse power, P_0, and the sample ablation threshold intensity, I_{th}, is easily derived [13]:

$$I_{\text{th}} = \frac{P_0}{e\pi\rho_{\max}^2} \cong 0.117\frac{P_0}{\rho_{\max}^2}. \tag{1}$$

If the profile etched in the sample does not exhibit the two lobes, a new scan should be done increasing the pulse power (energy), or using a tighter focusing lens (that decreases the beam waist w_0 and, consequently, reduces P_{crit}), so the lobes are created. The lobes maximum half width $\rho_{\max}$ occurs at the positions [13] $\pm\chi = z_0[(2P_0)/(e\pi w_0^2 I_{\text{th}}) - 1]^{1/2}$ where the pulse intensity is always $(1/2)eI_{\text{th}} \approx 1.36I_{\text{th}}$, thus not depending on the beam waist size w_0 or the confocal parameter z_0. To determine the ablation threshold intensity, only the pulse power must be known, and all other geometrical parameters of the beam

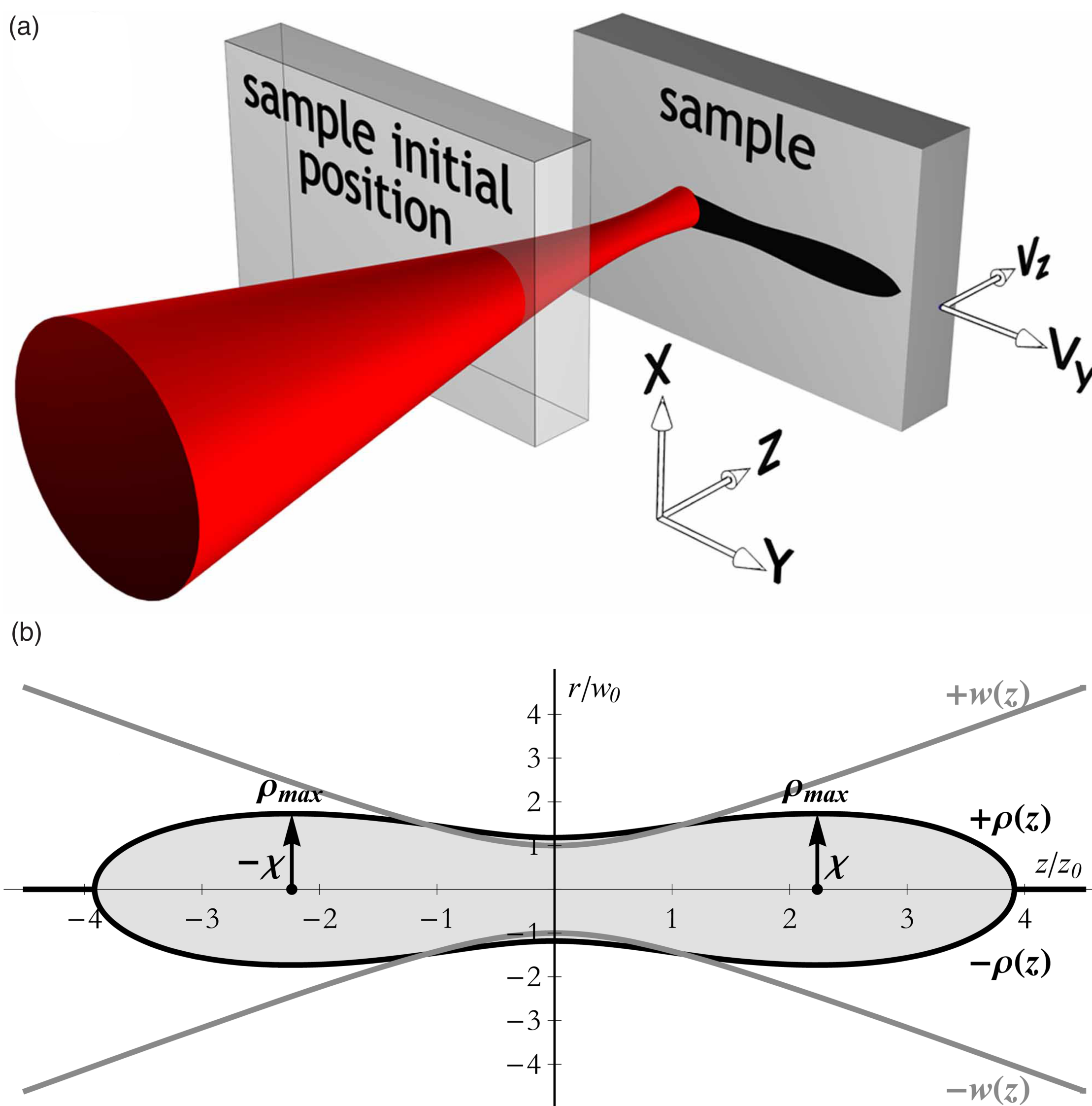

Fig. 1. (Color online) Diagonal scan method: a) scheme of the experimental setup showing the sample movement and b) profile of the sample surface etching, $\rho(z)$, by the laser beam, $w(z)$ for $P_0 = 6P_{\text{crit}}$. The vertical and longitudinal axes are normalized by the beam waist w_0 and confocal parameter z_0, respectively.

(focusing lens, beam waist, and propagation law) can be left undetermined. The measurement of the ablation profile maximum half width and the use of Eq. (1) determine the ablation threshold intensity I_{th}. Multiplying this value by the pulse duration gives the ablation threshold fluence, F_{th}.

We applied the D-scan method to determine the ablation threshold of four samples: a pure LiSAF crystal and two 1% Cr^{3+} doped Cr:LiSAF samples, all grown in our crystal growth laboratory, and a 1.5% Cr^{3+} sample extracted from a crystal rod grown by VLOC [16]. To etch the profiles in the samples, an amplified Ti:sapphire laser system was used generating 18.9 ps (FWHM) pulses, centered at 830 nm, at 1 kHz repetition rate, and the beam was focused by a 20 cm converging lens. The samples were fixed to an x-y-z translation table controlled by a computer and were moved diagonally to the laser beam by $y = 10$ mm and $z = 60$ mm through its waist at constant speeds $v_y = 1$ mm/s and $v_z = 6$ mm/s. Five ablation profiles were etched in each sample at different pulse energies always vertically apart by 500 μm [x direction in Fig. 1(a)]. The samples were photographed under an optical microscope, and the photographs were used to measure ρ_{max} using the 500 μm vertical separation as scale for each profile and to determine the ablation thresholds.

3. Results

Figure 2(a) shows the ablation profiles etched in the pure LiSAF sample. In all five profiles the two lobes can be observed, although there is an asymmetry around the central position. The right portions of the profiles were ablated after the sample crossed the beam waist, and since the experiments were done in air, we attribute the profile asymmetry to nonlinear effects that occur near the focus position, modifying the beam characteristics. For this reason, we chose to measure the maximum transversal dimension of the profile in its left portion (corresponding to the sample positioned before the beam waist), where nonlinear effects that modify the beam shape are minimized. For all the other Cr^{3+} doped samples, the results were similar. Table 1 presents for each profile of Fig. 2(a) the value measured for ρ_{max}, the pulse energy ε_p, and the ablation threshold fluence F_{th} calculated using Eq. (1) and 18.9 ps for the pulse's duration. The average value of the ablation threshold fluence measured is (1.61 ± 0.11) J/cm^2. In Fig. 3 the ablation threshold fluences measured for all samples are shown as a function of the Cr^{3+} concentration (the average value of the fluences measured for the two 1% Cr^{3+} doping samples is shown), and it can be observed that the ablation threshold decreases with the Cr^{3+} concentration raise. This is an expected result, since the insertion of a dopant in the host causes defects that usually create energy levels in the bandgap, consequently decreasing the energy needed to generate the initial free electrons by the multiphoton or tunneling processes. Besides, the dopant introduction in the crystal matrix distorts the crystal structure, creating local stresses that degrade the host mechanical properties. The unexpected result is that the higher Cr^{3+} concentration (1.5 mol. %) sample has a higher ablation threshold than the 1 mol. % samples. However, the lower Cr^{3+} content samples grown at our laboratories have not gone through an annealing process, which would reduce mechanical stresses remaining from the growth process. The higher Cr concentration sample (grown by VLOC), has probably passed through an annealing process, as is usually done in laser gain media, minimizing tensions and increasing the ions' bond energies to the structure, which is what improves the crystal mechanical properties [17]. This additional energy results in an increase in the ablation threshold.

Due to the LiSAF crystal transparency, it was possible, under the optical microscope, to take a photograph of the lateral view of profile 1 shown in Fig. 2(a) [observation through face yz, Fig. 1(a)], presented in Fig. 2(b). The ablation depth dependence on the distance, $h(z)$, was measured in this picture, and the >total width, $2\rho(z)$, of the ablation profile was determined from Fig. 2(a). From these data it was possible to calculate an ablation effective volume, $V_{eff}(z)$, defined by

$$V_{eff}(z) = \rho(z)^2 h(z), \tag{2}$$

that depends on the sample position, and consequently, on the pulse's intensity. The results are

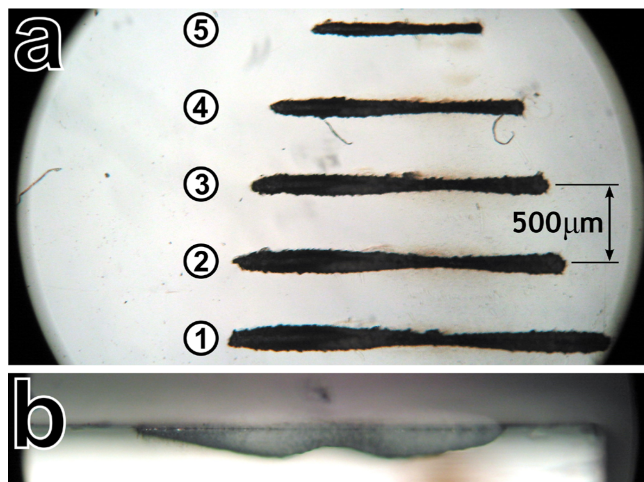

Fig. 2. (Color online) a) Optical microscope picture of the profiles etched in the pure LiSAF sample surface at different energies and b) lateral picture of profile 1.

Table 1. Pure LiSAF Sample Fluence Ablation Thresholds

Profile	ρ_{max} (μm)	ε_p (μJ)	F_{th} (J/cm^2)
1	79.8 ± 4.9	814 ± 9	1.50 ± 0.18
2	73.1 ± 4.8	723 ± 11	1.58 ± 0.21
3	64.3 ± 4.7	587 ± 8	1.66 ± 0.25
4	55.4 ± 4.6	447 ± 8	1.71 ± 0.29
5	42.1 ± 4.6	279 ± 6	1.84 ± 0.11

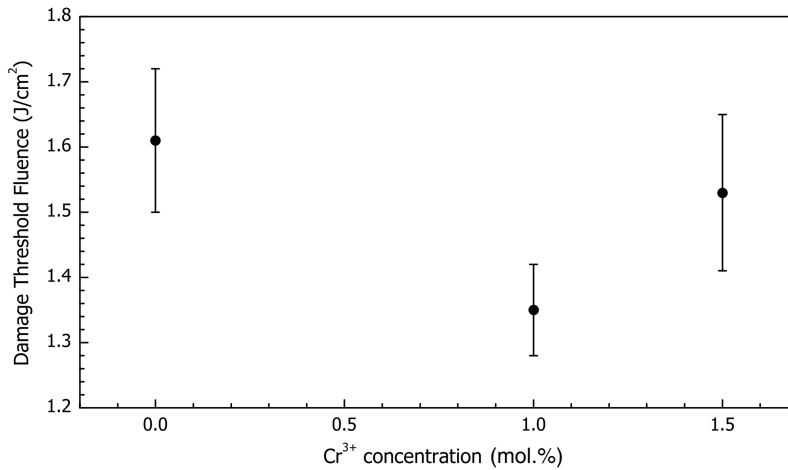

Fig. 3. Cr:LiSAF ablation threshold dependence on the Cr^{3+} concentration.

shown in Fig. 4, where it can be clearly seen that the maximum material removal rate per pulse occurs away from the beam waist. The maximum V_{eff} occurs near the maximum width of the profile, ρ_{max}, and has the value $(1.12 \pm 0.11)10^6\,\mu\text{m}^3$. Near the beam waist, V_{eff} presents a local minimum, with the value $(150 \pm 34)10^3\,\mu\text{m}^3$. The ratio of these values is 7.5, demonstrating that, in this temporal regime, the maximum material removal rate takes place away from the beam focus, being almost an order of magnitude greater than at the beam waist. The minimum V_{eff} value around the waist position is a consequence of the small beam size and the small ablation depth. We propose that the high laser intensity at the beam waist generates a huge electron density that shields the beam, minimizing the laser penetrating depth. Two processing conditions are now defined: one at the beam focus, where lateral and depth precisions are enhanced due to the small material removal rate, and the other away from the focus, where the material removal rate per pulse is maximized. Contrary to what is intuitively expected, in this temporal regime, etching a sample at the beam waist does not ensure the maximum ablation depth or maximum material removal rate per pulse.

4. Conclusions

We applied a new and simple method that does not require precise knowledge of the laser beam geometry to determine the ablation threshold of Cr:LiSAF samples in the ultrashort pulse regime. The method only demands the sample under investigation to be

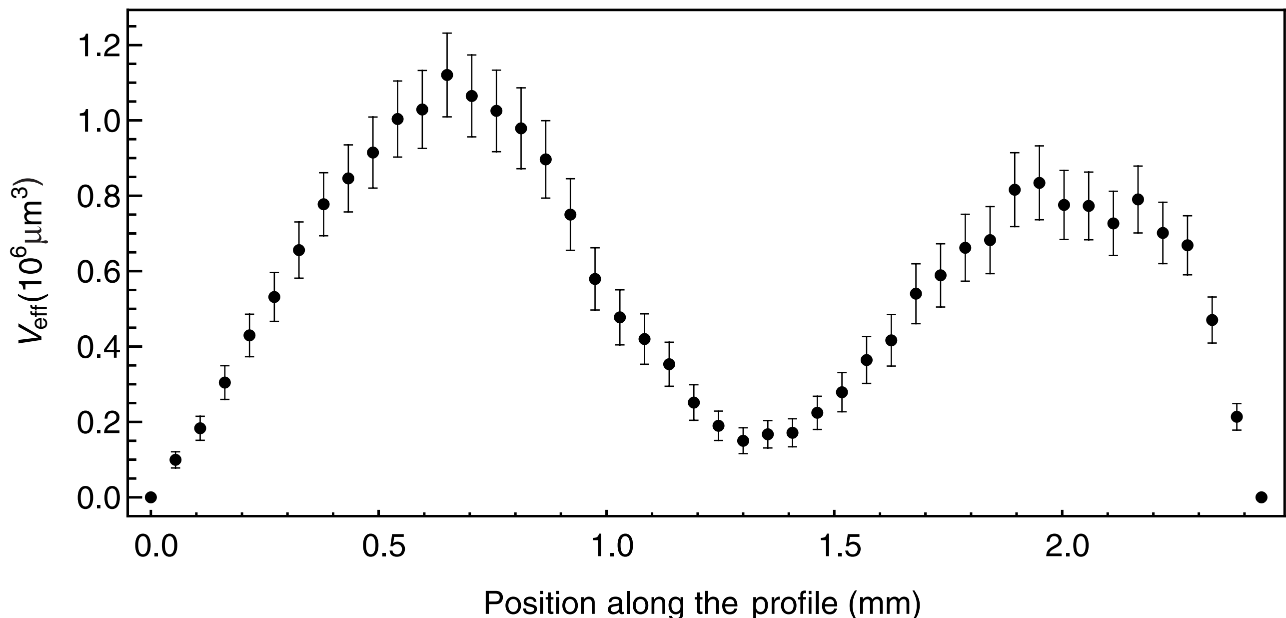

Fig. 4. Effective volume ablated dependence on the sample surface along the ablation profile.

diagonally scanned across the focused laser beam waist, etching a profile in its surface, and the measurement of the maximum half width of this profile. In the samples investigated, a decrease in the ablation threshold was observed with the Cr^{3+} concentration increase, and this can be explained by residual absorption and mechanical stress, both resulting from the Cr^{3+} introduction on the crystal. In addition, the transparency of the sample allowed the lateral observation of the etched profile giving access to the ablation depth, which permitted the calculation of effective ablated volume. This effective volume dependence on the laser intensity led us to determine that the maximum material removal rate occurs away from the beam waist.

The authors acknowledge the financial support received from FAPESP (grant 00/15135-9) and FINEP.

References

1. N. Bloembergen, “Laser-induced electric breakdown in solids,” IEEE J. Quantum Electron. **10**, 375–386 (1974).
2. D. Du, X. Liu, G. Korn, J. Squier, and G. Mourou, “Laser-induced breakdown by impact ionization in SiO_2 with pulse widths from 7 ns to 150 fs,” Appl. Phys. Lett. **64**, 3071–3073 (1994).
3. M. D. Perry, B. C. Stuart, P. S. Banks, M. D. Feit, V. Yanovsky, and A. M. Rubenchik, “Ultrashort-pulse laser machining of dielectric materials,” J. Appl. Phys. **85**, 6803–6810 (1999).
4. W. Kautek, J. Kruger, M. Lenzner, S. Sartania, C. Spielmann, and F. Krausz, “Laser ablation of dielectrics with pulse durations between 20 fs and 3 ps,” Appl. Phys. Lett. **69**, 3146–3148 (1996).
5. L. V. Keldysh, “Ionization in the field of a strong electromagnetic wave,” Sov. Phys. JETP **20**, 1307–1314 (1965).
6. M. Lenzner, J. Kruger, S. Sartania, Z. Cheng, C. Spielmann, G. Mourou, W. Kautek, and F. Krausz, “Femtosecond optical breakdown in dielectrics,” Phys. Rev. Lett. **80**, 4076–4079 (1998).
7. M. Uiberacker, T. Uphues, M. Schultze, A. J. Verhoef, V. Yakovlev, M. F. Kling, J. Rauschenberger, N. M. Kabachnik, H. Schroder, M. Lezius, K. L. Kompa, H. G. Muller, M. J. J. Vrakking, S. Hendel, U. Kleineberg, U. Heinzmann, M. Drescher, and F. Krausz, “Attosecond real-time observation of electron tunnelling in atoms,” Nature **446**, 627–632 (2007).
8. A. P. Joglekar, H. Liu, G. J. Spooner, E. Meyhofer, G. Mourou, and A. J. Hunt, “A study of the deterministic character of optical damage by femtosecond laser pulses and applications to nanomachining,” Appl. Phys. B **77**, 25–30 (2003).
9. M. Bass and D. W. Fradin, “Surface and bulk laser-damage statistics and the identification of intrinsic breakdown processes,” IEEE J. Quantum Electron. **9**, 890–896 (1973).
10. S. Nolte, C. Momma, H. Jacobs, A. Tunnermann, B. N. Chichkov, B. Wellegehausen, and H. Welling, “Ablation of metals by ultrashort laser pulses,” J. Opt. Soc. Am. B **14**, 2716–2722 (1997).
11. E. G. Gamaly, A. V. Rode, B. Luther-Davies, and V. T. Tikhonchuk, “Ablation of solids by femtosecond lasers: ablation mechanism and ablation thresholds for metals and dielectrics,” Phys. Plasmas **9**, 949–957 (2002).
12. J. M. Liu, “Simple technique for measurements of pulsed Gaussian-beam spot sizes,” Opt. Lett. **7**, 196–198 (1982).
13. R. E. Samad and N. D. Vieira, “Geometrical method for determining the surface damage threshold for femtosecond laser pulses,” Laser Phys. **16**, 336–339 (2006).
14. M. Ruiz, E. A. Barbosa, E. P. Maldonado, S. P. Morato, N. U. Wetter, N. D. Vieira, and S. L. Baldochi, “Zone melting growth of $LiSrAlF_6$:Cr crystals for diode laser pumping,” J. Cryst. Growth **241**, 177–182 (2002).
15. S. L. Baldochi and S. P. Morato, “Fluoride bulk crystals growth,” in *Encyclopedia of Materials: Science and Technology*, K. H. J. Buschow, R. W. Cahn, M. C. Flemings, B. Ilschner, E. J. Kramer, and S. Mahajan, eds. (Pergamon, 2001), pp. 3200–3205.
16. VLOC, retrieved http://www.vloc.com/vlochome.htm.
17. J. J. De Yoreo, L. J. Atherton, and D. H. Roberts, “Elimination of scattering centers from Cr:$LiCaAlF_6$,” J. Cryst. Growth **113**, 691–697 (1991).